Stability of the flow in a soft tube deformed due to an applied pressure gradient

M. K. S. Verma and V. Kumaran

Department of Chemical Engineering, Indian Institute of Science, Bangalore 560 012, India
(Received 31 October 2014; revised manuscript received 14 February 2015; published 3 April 2015)

A linear stability analysis is carried out for the flow through a tube with a soft wall in order to resolve the discrepancy of a factor of 10 for the transition Reynolds number between theoretical predictions in a cylindrical tube and the experiments of Verma and Kumaran [J. Fluid Mech. **705**, 322 (2012)]. Here the effect of tube deformation (due to the applied pressure difference) on the mean velocity profile and pressure gradient is incorporated in the stability analysis. The tube geometry and dimensions are reconstructed from experimental images, where it is found that there is an expansion and then a contraction of the tube in the streamwise direction. The mean velocity profiles at different downstream locations and the pressure gradient, determined using computational fluid dynamics, are found to be substantially modified by the tube deformation. The velocity profiles are then used in a linear stability analysis, where the growth rates of perturbations are calculated for the flow through a tube with the wall modeled as a neo-Hookean elastic solid. The linear stability analysis is carried out for the mean velocity profiles at different downstream locations using the parallel flow approximation. The analysis indicates that the flow first becomes unstable in the downstream converging section of the tube where the flow profile is more pluglike when compared to the parabolic flow in a cylindrical tube. The flow is stable in the upstream diverging section where the deformation is maximum. The prediction for the transition Reynolds number is in good agreement with experiments, indicating that the downstream tube convergence and the consequent modification in the mean velocity profile and pressure gradient could reduce the transition Reynolds number by an order of magnitude.

I. INTRODUCTION

Advances in microfabrication have made possible the miniaturization of complex reaction networks onto "lab-on-a-chip" devices, in which the reactors and channels have dimensions less than 1 mm. Miniaturization has several potential benefits, such as fast reactions in controlled environments with small volumes of reagents in devices of small size. However, reactions take place only when the reactant streams mix at the molecular level, and it has long been recognized that slow mixing could be a bottleneck in microreactors [1,2]. At the small length scales and low velocities used in microfluidics, flows are laminar and mixing takes place due to molecular diffusion. The time required for mixing across a length scale A can be estimated as A^2/D, where D is the molecular diffusion coefficient. The diffusion coefficient for small molecules in liquids is of the order of 10^{-9} m^2/s, while that for complex and polymeric molecules could be up to four orders of magnitude lower. Based on this, the time required for diffusion across a channel of width 1 mm is in the range $10^3 - 10^7$ s. Such long mixing times adversely affect the feasibility of sample preparation processes in microfluidic devices.

A promising method for enhancing mixing in microfluidic devices [3,4] is to make the walls of the microconduit sufficiently soft, so the laminar flow is disrupted by a flow instability due to a dynamical coupling between the fluid and the soft wall. This instability occurs at a Reynolds number (or flow velocity) much lower than that for the flows in rigid tubes or channels. Here the Reynolds number $\mathrm{Re} = \rho V A/\mu$ is the ratio of inertial and viscous stresses, ρ is the fluid density, A is the characteristic length (tube diameter or channel height), V is the average velocity, and μ is the fluid viscosity. While the experimental results for soft-wall instability in a microchannel are in agreement with theoretical predictions [4], there is still

a difference of a factor of about 10 between the theoretical predictions and experimental results for the flow in a soft tube [3]. The resolution of this discrepancy is the subject of the present analysis.

The understanding developed for stability or laminar-turbulent transition in rigid-walled channels and tubes cannot be directly applied to the flow through soft conduits. In rigid tubes and channels, the transition is not predicted by the a linear stability analysis of the laminar flow. For a two-dimensional channel, the transition is observed in experiments at a Reynolds number of about 1200 [5], while the linear stability studies [6] predict that the flow becomes unstable at a Reynolds number of 5772. In a rigid pipe, the transition is observed at a Reynolds number of about 2100, whereas the linear stability analysis predicts that the flow is stable at all Reynolds numbers. There is now a consensus that the laminar-turbulent transition in rigid conduits is due to a highly subcritical bifurcation which is certainly three dimensional, though the exact nature of the transition is still not completely understood.

The stability of flow in channels or tubes with flexible walls, made of viscoelastic solids of finite thickness, qualitatively differs from those in rigid conduits, due to the dynamical coupling between the velocity fluctuations in the fluid and the displacement fluctuations in the wall material. It has been shown, in previous linear stability studies, that the flow could become unstable at a transition Reynolds number which depends on the scaled shear modulus of the wall material. There is an instability even at zero Reynolds number, when the dimensionless number $V\mu/GA$ increases beyond a critical value [7,8], where μ is the fluid viscosity, G is the elasticity modulus of the wall material, and V and A are the characteristic flow velocity and length. The instability is caused by the transfer of energy from the mean flow to the fluctuations due to the shear work done at the interface. The transition

Reynolds number does depend on the specific type of wall material [9–13]. Weakly nonlinear studies [14,15] indicate that the low-Reynolds-number instability is subcritical. There is experimental confirmation of the zero-Reynolds-number instability [16,17], and nonlinear oscillatory states have been sustained even after transition [18]. It has been shown that the mass transfer rates near the elastic surface are enhanced by up to 25% due to the elastohydrodynamic instability [19].

Other mechanisms of instability at high Reynolds number also qualitatively differ from the instability for the flow past a rigid surface. Viscous effects are negligible in the bulk of the flow in the high-Reynolds-number "inviscid" instability [20–22], though they are significant in boundary layers of thickness $\text{Re}^{-1/2}$ at the walls. The transition Reynolds number follows the scaling $\text{Re}_t \propto \Sigma^{1/2}$, where the dimensionless number $\Sigma = \rho G A^2/\mu^2$ does not depend on the flow velocity and depends only on the material properties and geometry. The transition is due to the destabilising effect of inertial stresses within the bulk of the flow. The destabilizing mechanism in the "wall-mode" instability [22–24], which is the transfer of energy from the mean flow to the fluctuations due to the shear work at the interface, is identical to that for the viscous instability. The viscous stress perturbations are important in a wall layer of thickness $\text{Re}^{-1/3}$ at the wall, and the transition Reynolds number scales as $\text{Re}_t \propto \Sigma^{3/4}$. Weakly nonlinear studies have shown that the wall-mode instability is supercritical [15], in contrast to the low-Reynolds-number instability, which is subcritical [10]. The transition Reynolds number for the inviscid and wall-mode instabilities are relatively insensitive to the wall constitutive relation, provided the transition Reynolds number is higher than about 10.

Weakly nonlinear studies of the wall-mode instability indicate that the primary bifurcation is supercritical, in contrast to the subcritical bifurcation in the flow through rigid tubes and channels. In addition to the theoretical indications, in experiments [3], there is evidence that the transition is preceded by a linear instability of the base parabolic flow. In dye-stream experiments where a dye stream is introduced at the center of the tube of the tube, it is observed that the perturbations of the dye stream just above the critical Reynolds number are of well-defined frequency after transition, and the amplitude of perturbations increases continuously as a function of the control parameter which is the difference between the Reynolds number and the transition Reynolds number. This is in contrast to a discontinuous breakup of the dye stream that is observed in the transition in a rigid tube. All of these indicate that the mechanism of transition is a linear instability and not the nonlinear growth of perturbations in the vicinity of a highly subcritical transition. Therefore, we restrict attention to the linear stability analysis in the present study.

In the experimental studies on the flow through a flexible tube [3], it was found that the transition Reynolds number is lower, by about an order of magnitude, in comparison to theoretical predictions. It was speculated that the reason for the low transition Reynolds number could be the tube deformation due to the applied pressure difference. The pressure gradient results in an expansion of the tube near the inlet and then a decrease in radius as the pressure decreases towards the outlet. In that case, it was observed that the flow is destabilized not in the diverging section where the slope of the wall is largest but in the converging section where the slope of the wall is relatively smaller. Based on qualitative arguments relating the slope to the pressure gradient, the relation $\text{Re}_t \propto \Sigma^{5/8}$ for the transition Reynolds number was recovered.

Experiments for transition in a microchannel of rectangular cross section with height (smallest dimension) 100 μm [4] indicated that the transition Reynolds number in that case could be as low as 200. The transition Reynolds number was found to scale as $\text{Re}_t \propto \Sigma^{5/8}$ in that case as well, where Re_t and Σ are based on the height of the microchannel. The effect of deformation in the flow through a microchannel was incorporated in a linear stability analysis [4], and it was found that there is a modification of the velocity profile and the pressure gradient due to the channel deformation. In the converging section of the channel, the transition Reynolds number was lower, by a factor of about 10, in comparison to the flow through an channel with flat walls. Here, we carry out the linear stability analysis for the flow through a tube to determine whether there is a similar reduction in the transition Reynolds number.

One of the defining features of the stability of parallel shear flows is that the characteristics of the flow in channels and tubes completely differ. In a channel, there is the Tollmien-Schlichting instability that destabilizes the flow at a Reynolds number of about 5772 [6]. In contrast, in a tube flow, the linear stability analysis indicates that the flow is always stable at all Reynolds numbers. This difference is due to the difference in the nature of the differential operators in the Cartesian and cylindrical coordinates when we write down the Orr-Sommerfeld equations. The instability in the flow through a microchannel bounded by a soft wall [4] also cannot be used to draw conclusions for the flow through a soft tube. In the earlier experiments [4], only one of the walls was soft, while the other three were rigid. Due to this, symmetry about the central plane was already broken in the base state, even when we use a parallel flow approximation. Therefore, it is not surprising to find an instability. In the present tube flow, the base configuration is axisymmetric, and so there is no symmetry breaking about the axis in the base state when we use the near-parallel approximation. Consequently, it is not clear whether the same mechanism of instability will apply for the flow through a soft tube as well.

Here a combination of flow simulations for reconstructing the laminar flow and stability analysis is used to examine the physical reason for the destabilization of the laminar flow. The laminar velocity profiles are reconstructed using two techniques, the ANSYS-FLUENT 13.0.0 software and the finite-difference formulation of Sutterby [25] for axisymmetric flows. The results of the two were found to be in agreement to within 1%, thus verifying the consistency of the flow profiles obtained by the two methods. In order to account for the tube deformation in the theory, the detailed shape of the tube and the variation in the radius in the streamwise direction are reconstructed from images recorded during the experiment. This detailed shape is used in a flow simulation in order to predict the pressure drop and the velocity profile within the channel.

In the flow simulation, we consider the flow of an incompressible Newtonian fluid in a conduit with the deformed cross section obtained from the experiments, while the wall

is modeled as an incompressible neo-Hookean solid with constant shear modulus. Gradients in the shear modulus created during the curing of the gel have been reported, and these do have a modest effect on the stability boundaries at low Reynolds number [26]. These gradients were not measured directly in the experiments of Verma and Kumaran [3], and there were no visible variations in the texture in the scanning electron microscope images of tube cross sections, and so we do not consider these gradients in the present analysis.

After reconstructing the velocity profile, we conduct a linear stability analysis to determine whether the velocity profile is stable or unstable. It is not feasible to use the same computational procedure for the linear stability analysis as for the base flow. For flows through a rigid pipe, computational fluid dynamics simulation packages such as ANSYS-FLUENT will predict a laminar velocity profile even when the Reynolds number is higher than the transition Reynolds number, because the laminar solution is a valid solution of the Navier-Stokes equations at all Reynolds numbers, and the transition is highly subcritical. In two-dimensional or axisymmetric computations, the turbulent profile is obtained only when a turbulence model is used. In fact, even for three-dimensional direct numerical simulation computations in a channel or tube, the flow will be laminar when the Reynolds number exceeds the transition Reynolds number. It is necessary to impose relatively large perturbations on the flow profile in order to get to the turbulent state close to the transition Reynolds number.

In the flow through the deformable tube, the ANSYS-FLUENT simulations as well as the finite-difference computations capture only the laminar velocity profiles, since these are solutions of the Navier-Stokes equations, albeit unstable solutions. For the unstable modes, experiments indicate that the frequency is of the order of 10^2-10^3 s^{-1}. Even if we were to impose perturbations on the base laminar flow, it is infeasible to capture such high-frequency perturbations in finite-difference schemes that are integrated in time, since they require unrealistically short time steps. Therefore, we have evaluated the base state using the ANSYS-FLUENT simulations and the finite-difference formulation and then carried out the stability analysis of this base state.

In the linear analysis, we use a local parallel flow approximation but use the velocity and pressure profiles from the flow simulations as inputs. The results of the linear stability analysis are compared with experimental results of Verma and Kumaran [3]. The analysis is restricted to axisymmetric perturbations for two reasons. First, the experiments indicate that the wall deformation and wall motion are axisymmetric. Second, there is a previous linear stability study [27] which shows that axisymmetric disturbances are more unstable than nonaxisymmetric disturbances for the flow in a converging tube.

The analysis is presented as follows.

(1) The flow geometry and its determination from the experimental results are discussed in Sec. II. Measurements from the experiments (Fig. 1) are used to reconstruct the downstream variation of the tube radius (A) as function of the downstream distance z, as shown in Fig. 2.

(2) The fluid flow solutions in the deformed tube with no-slip boundary conditions at the wall are determined in Sec. III A, starting from the Navier-Stokes equations. This was done in two ways—the first is using the ANSYS-FLUENT software, and

the second is using the numerical method of Sutterby [25]; the results from the two procedures are in agreement. The inertial terms are included in the flow computation due to the variation in the wall diameter. Though the slope of the wall α is numerically small, as shown in Fig. 11, the inertial terms in the momentum conservation equation scale as Reα, which is not small in the present system.

(3) Section III B provides the base-state solution for the displacement field in the wall material. In this, we have made the locally parallel approximation for the displacement field and evaluated the displacement field from the fluid pressure and stress at the fluid-solid interface. Since the solid is stationary in the base state, there are no inertial terms, and the momentum conservation equation just reduces to the solenoidal condition on the stress in the solid. Since the slope of the wall is numerically small as shown in Fig. 11, the parallel approximation is used for the displacement field.

(4) The linear stability analysis is formulated in Sec. III C. Here, the mean velocity profile and pressure gradient in the fluid, and the mean displacement profile in the solid wall, are used, together with the parallel flow approximation, to determine the stability limits. The inertial terms in the fluid momentum equation and the acceleration in the solid momentum equation are included in the linear stability analysis. The parallel flow approximation is valid only when the length scale for the flow variation in the streamwise direction, which is comparable to the ratio of the tube radius and the slope of the wall, is much larger than the wavelength of the perturbations. The wavelengths of the most unstable modes computed in Figs. 8, 9, and 10 are compared with the ratio of the ratio of the tube radius and wall slope shown in Fig. 11 to verify that the conditions required for the parallel flow approximation are satisfied.

(5) The results are discussed in Sec. IV, where the predictions of the linear stability analysis are compared with experimental results, and the physical mechanism of destabilization is examined in greater detail.

II. FLOW GEOMETRY

The experiments of Verma and Kumaran [3] were carried out in a tubular bore of diameters 0.8 and 1.2 mm within a polydimethyl siloxane (PDMS) block of square cross section with height 10 mm, as shown in Fig. 1(a). The experimental tube consists of a hard "developing" section of length 10 cm, fabricated using gel with shear modulus 0.5 MPa, which is sufficiently high that there is no reduction in the transition Reynolds number below the rigid tube value of 2100. The length of the development section is sufficient for the development of a parabolic profile and for inlet disturbances to be damped out. The development section is followed by a "test" section of length 9.5 cm made of soft gel with a lower catalyst concentration to obtain a sufficiently low shear modulus that there is a reduction in the transition Reynolds number below the rigid tube value of 2100. Experiments were carried out for three different shear moduli in the test section, 18 kPa, 25 kPa, and 35 kPa. The development and test sections are seamlessly bonded, and there is a pressure port just upstream of the entrance to the test section to measure the pressure drop across the tube. The deformation of the tube as a function of downstream distance in the test section was
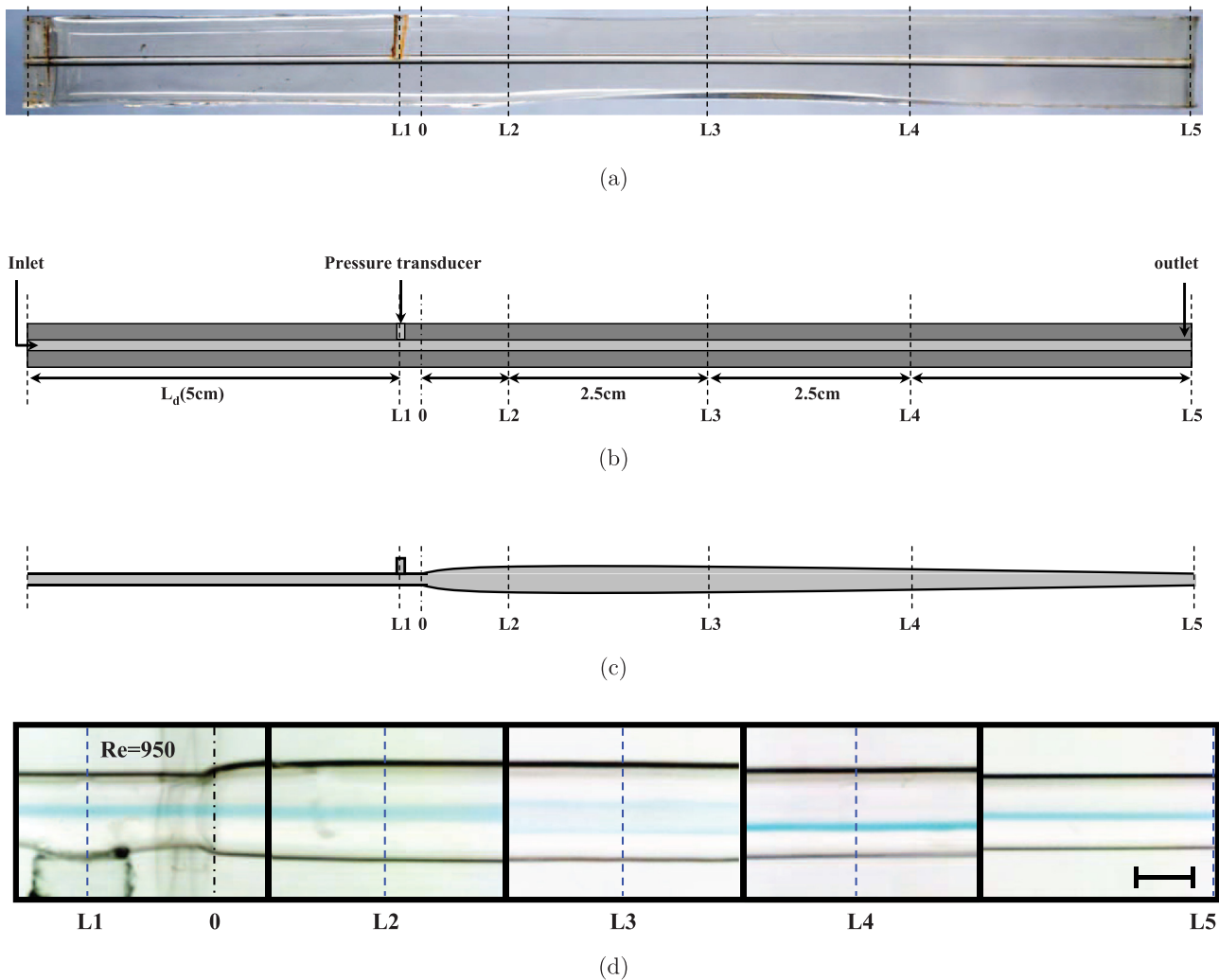
FIG. 1. (Color online) Undeformed tube of diameter 1200 μm (a), schematic of undeformed tube (b) and deformed tube (c), and close-up views of deformed tube where the soft section is made of PDMS with shear modulus 18 kPa, at a Reynolds number of 950 (d). The locations are $L_1 = 2$ mm upstream, and $L_2 = 1$ cm, $L_3 = 3.5$ cm, $L_4 = 6$ cm, and $L_5 = 9.5$ cm downstream of the entrance to the soft section. The scale bar in the figures is 1 mm in length. Panels (a) and (d) are reproduced from Verma and Kumaran [3].

measured using cameras mounted above and on the side of the PDMS block. An example of images of a deformed tube used for measurements is shown in Fig. 1(d), and the reconstruction of the tube deformation is shown in Fig. 1(c).

Transition was inferred using three different measurement techniques. The first is the dye-stream measurement, where dye is injected at the center of the tube, and images are captured of the progress of the dye stream through the tube, as shown in Fig. 1(d). The dye stream is straight and undisturbed in a laminar flow, while there is a spontaneous breakup of the dye stream in a turbulent flow. The second measure is the friction factor obtained from the pressure difference across the soft section. In the flow through soft tubes, breakup of the dye stream was observed at a Reynolds number as low as 500 for the softest materials used, which is much smaller than the rigid tube value of 2100. Motion of the viscoelastic wall was also inferred by laser scattering from the curved interface between the solid and the fluid. From a video of the laser scattering off the wall of the tube, the average and the mean square of the fluctuations in the gray-scale intensity were calculated. It

was observed that at the Reynolds number where transition is observed in the dye stream, there is also a sharp increase in the mean square of the laser intensity fluctuations, signifying the onset of wall motion.

In the experimental study of Verma and Kumaran [3], the tube deformation was taken into account in the friction factor and Reynolds number by defining an "average" diameter across the tube. Here we determine the variation in the velocity profiles along the length of the tube, and so there is no necessity of defining an average diameter. The flow Reynolds numbers are, in all cases, reported in terms of the average velocity $(Q/\pi A_0^2)$ and the undeformed tube diameter $2A_0$, $\mathrm{Re} = 2\rho Q/\pi A_0 \mu$, where Q is the flow rate. The friction factor calculated from the pressure drop measurements was found to depart from the laminar value of 16/Re at the same Reynolds number where the dye-stream breakup was observed.

The flow geometry is a deformed axisymmetric tube with a straight axis, in which the radius is a function of position. The streamwise and radial coordinates are z and r, respectively, and the configuration and flow are considered axisymmetric
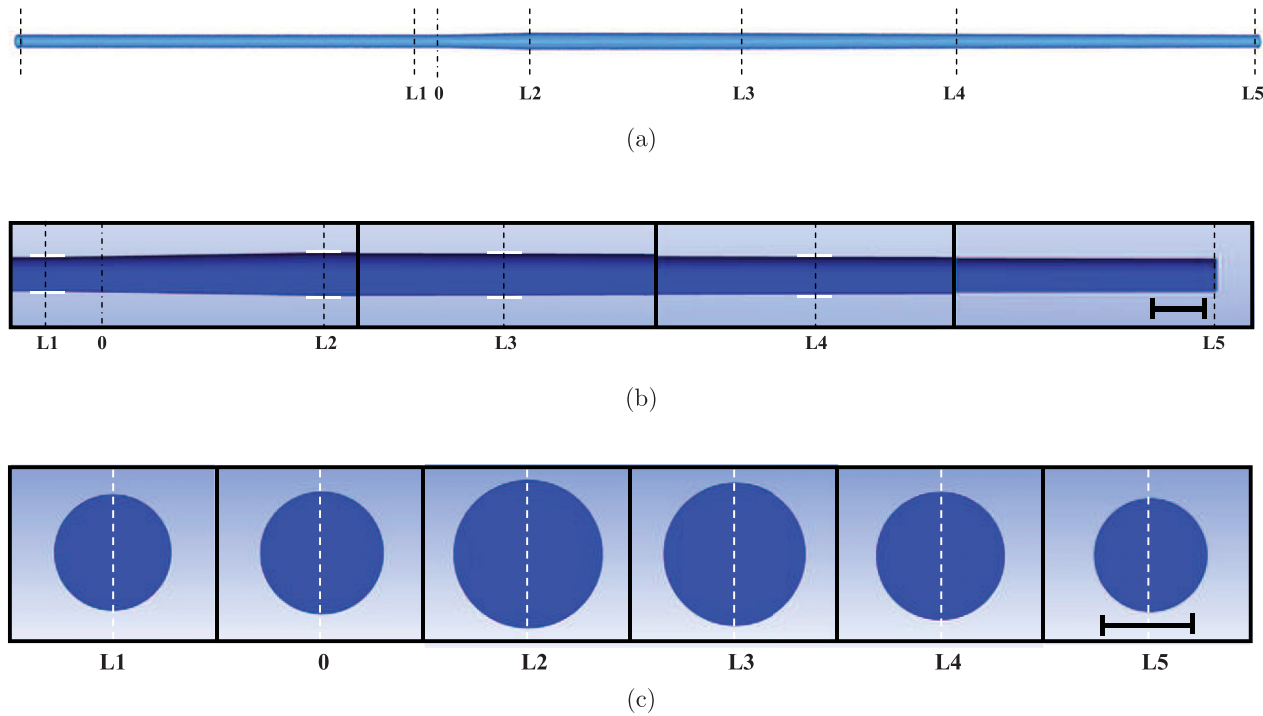
FIG. 2. (Color online) The side view (a) and the magnified side view at different streamwise locations (b) and the cross-sectional view (c) at different streamwise locations of the tube reconstructed from the experimental images in Fig. 1 with soft walls made with shear modulus 18 kPa at Reynolds number 950. The locations are $L_1 = 2$ mm upstream and $L_2 = 1$ cm, $L_3 = 3.5$ cm, $L_4 = 6$ cm, and $L_5 = 9.5$ cm downstream of the entrance to the soft section. The scale bar in the figures is 1 mm.

so there is no variation in the meridional direction. The pressure gradient along the length of the tube deforms the tube wall in the soft section, resulting in an axial variation in the tube radius (the undeformed tube diameter is 1200 μm). The deformation along the length of the tube was measured using a camera on the side. The deformed tube geometry is reconstructed by a cubic spline interpolation of the tube radius at different locations. Figures 2(a) and 2(b) show the side view of the reconstructed tube corresponding to the deformed tube in Fig. 1(d) at different streamwise locations. The cross section at different locations are shown in Fig. 2(c). This tube geometry is used to obtain the velocity and pressure drop using computational fluid dynamics.

The shape of the solid wall, which is a gel block with square cross section of side 10 mm with a tubular bore of diameter 1.2 mm removed from the axis, is quite complex. In the stability analysis, the soft wall is approximated as an annulus with inner radius A and outer radius equal 6 mm, which enables us to carry out a linear stability analysis using an axisymmetric coordinate system. This is not a severe approximation, because the outer radius of the block in the simulation is at least 10 times larger than the inner radius. Fluctuations in the displacements in the annular region are significant only over distances comparable to the inner tube diameter, and they decrease to zero as the outer edge of the annulus is approached. Due to this, the variation in the transition Reynolds number predicted here is very small; there is an increase in the transition Reynolds number of about 2% for the softest gels when the outer diameter is decreased from 6 to 5 mm and a decrease of about 1% when the outer diameter is increased from 6 to 7 mm. The eigenfunctions for the solid displacement field in the wall, shown later in Fig. 12, con-

firm that the solid displacement field decreases to zero over a distance comparable to the radius of the inner bore, and the displacement fluctuations are small at the outer surface of the gel.

III. ANALYSIS

A. Base-state fluid flow

The system consists of a pressure-driven flow of an incompressible Newtonian fluid of density ρ and viscosity μ in a tube of radius A with a viscoelastic wall in the region $A \leqslant r \leqslant HA$, as shown in Fig. 3. A cylindrical coordinate
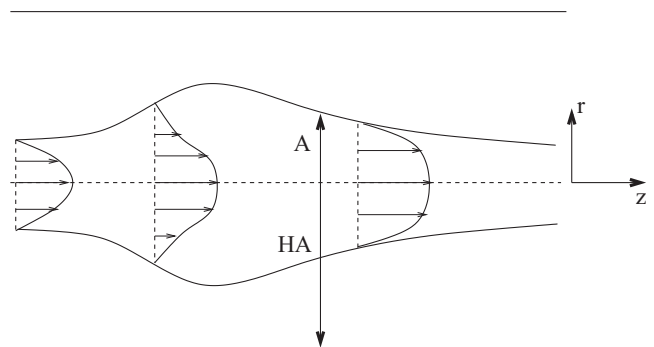
FIG. 3. Schematic diagram, not to scale, showing the coordinate system, the fluid and gel, local tube diameter A, and the outer diameter HA for the soft wall. A schematic of the parabolic profile at the entrance to the test section is shown on the left, and the qualitative variation in the velocity in the diverging and converging sections, plotted later in Fig. 4, are also shown.

system is used, where the flow is in the z direction and the velocity variation is in the radial r direction, and we consider the system to be axisymmetric so there is no variation in the θ direction. The annular wall is modelled as an incompressible elastic neo-Hookean solid of density ρ and shear modulus G. The densities of the solid and fluid are considered to be equal. Solid dissipation is neglected in the present analysis because previous studies [12] have shown that it does not have a significant effect on the flow stability at high Reynolds numbers greater than about 100, though solid dissipation does significantly affect the flow stability at low Reynolds number. The lengths are nondimensionalized by A, the velocities by GA/μ, and the pressure and stresses by G.

The mass and momentum conservation equations for the fluid are the usual incompressible Navier-Stokes equations,

$$\nabla \cdot \mathbf{v} = 0, \tag{1}$$

$$\frac{\text{Re}}{\Gamma} \left(\frac{\partial \mathbf{v}}{\partial t} + \mathbf{v} \cdot \nabla \mathbf{v} \right) = -\nabla p + \nabla^2 \mathbf{v}, \tag{2}$$

where the Reynolds number is $\text{Re} = \rho V A/\mu$, the parameter $\Gamma = V\mu/GA$, ρ and μ are the fluid density and viscosity, V is the characteristic velocity, and the factor Re/Γ appears on the left side because the pressure and shear stress are scaled by G, while the velocity is scaled by GA/μ. The boundary conditions at the wall of the deformed channel are the no-slip condition, that is, zero tangential and normal velocity, since the wall is stationary in the base state.

The deformed tube is reconstructed from the measurements of the variation of diameter with downstream distance [3] as discussed in Sec. II. Flow simulations are then carried out in this tube in two ways. The first was by using ANSYS-FLUENT 13.0.0 in order to determine the modification of the flow and pressure profiles due to tube deformation. The second was by using the finite-difference formulation of Sutterby [25] for axisymmetric flows. It was verified that there is good agreement between the predictions of the two simulations for the developing flow in a tube starting with a plug flow at the inlet, and the maximum difference in the velocity is less than 1% for the grid resolutions used here. Consequently, the results for the mean velocity and profiles reported here are from the ANSYS-FLUENT simulations.

In the ANSYS-FLUENT simulations, the pressure-velocity formulation was used for a Newtonian fluid, and no-slip conditions were used at the walls for the mean flow. The computational domain consisted of the entire tube of length 19.5 cm, including the hard and soft sections, and the tube was discretized with a spatial resolution of 1 mm in the axial direction and 100 μm in the radial direction. For example, the deformed tube shape shown in Fig. 2 was discretized using 1 827 674 nodes. The conditions at the ends of the tube are a constant velocity at the inlet and a constant pressure at the outlet. The flow in the development section does depend on the specific velocity profile imposed at the inlet, but the velocity profile and the pressure in the test section were not affected by the velocity profile at the entrance to the development section. The simulation was initialized with zero velocity everywhere, the system was allowed to evolve until steady state is reached, and the convergence limit was set at 10^{-4} in the residual

for the continuity equation (the limiting condition in most simulations) or 10^{-3} for the velocity equations.

B. Base-state solid displacement

The deformation in the solid is described by the displacement field $\mathbf{w}$, which is the displacement of material points about their equilibrium positions due to the applied stresses. A Eulerian description, where the unstressed coordinates are used as the reference, is used in the present analysis.

$$\mathbf{w}(\mathbf{X},t) = \mathbf{x}(\mathbf{X},t), \tag{3}$$

where $\mathbf{X}$ is the unstressed location of a material point at $\mathbf{x}$. The deformation tensor $\mathbf{F}$ is defined as

$$\mathbf{F} = \nabla_{\mathbf{X}} \mathbf{w}, \tag{4}$$

The Cauchy stress tensor for an incompressible solid, when scaled by the shear modulus G, is given by

$$\sigma = -p_s \mathbf{I} + \mathbf{F} \cdot \mathbf{F}^T. \tag{5}$$

For an incompressible solid where the volume is conserved, the determinant of the deformation tensor is 1,

$$\text{Det}(\mathbf{F}) = 1. \tag{6}$$

The momentum conservation equation states that the rate of change of momentum in the material is equal to the divergence of the stress,

$$\frac{\text{Re}}{\Gamma} \left(\frac{\partial^2 \mathbf{w}}{\partial t^2} \right) = \nabla_X \cdot \mathbf{P}, \tag{7}$$

where $\mathbf{P}$ is Piola-Kirchoff stress tensor defined in indicial notation as

$$P_{IJ} = F_{IK}^{-1} \sigma_{KJ}^e, \tag{8}$$

where σ_{IJ}^e is the Cauchy stress tensor. Inserting the Piola-Kirchoff stress tensor into the momentum conservation equation (7), we find

$$\frac{\text{Re}}{\Gamma} \frac{\partial^2 w_I}{\partial t^2} = \frac{\partial \left(p F_{JI}^{-1} \right)}{\partial X_J} + \frac{\partial F_{IJ}}{\partial X_J}. \tag{9}$$

The displacement field in the solid layer is obtained by solving the governing mass and momentum equations, (6) and (7). From Eq. (6), we find

$$\frac{\bar{w}_R}{R} \left(\frac{\partial \bar{w}_R}{\partial R} \frac{\partial \bar{w}_Z}{\partial Z} - \frac{\partial \bar{w}_R}{\partial Z} \frac{\partial \bar{w}_Z}{\partial R} \right) = 1. \tag{10}$$

The steady-state momentum equation for solid is

$$\nabla_X \cdot \bar{\mathbf{P}} = 0. \tag{11}$$

Using Eq. (8) for $\bar{\mathbf{P}}$ and Eq. (5) for σ, the steady-state momentum equation is

$$\frac{\partial}{\partial X_J} \left(-\bar{p}_s \bar{F}_{JI}^{-1} + \bar{F}_{IJ} \right) = 0. \tag{12}$$

The conservation equations are solved subject to the zero displacement condition, $\bar{w}_Z = Z$ and $\bar{w}_X = X$, at the outer surface $r = (H + 1)$, and the stress balance conditions at the fluid-solid interface,

$$\sigma_{RR} = \tau_{RR}, \tag{13}$$

$$\sigma_{RZ} = \tau_{RZ}, \tag{14}$$

where the normal stress τ_{RR} at the fluid-solid interface is the pressure, and the shear stress is the product of the viscosity and the wall strain rate $\dot{\gamma}_w$ obtained from the fluid velocity profile.

In the base state, the solutions for the displacement and pressure fields have the form

$$\bar{w}_Z = Z - \frac{1}{4}\frac{\partial \bar{p}}{\partial z}[(H+1)^2 - R^2]$$
$$+\left(\dot{\gamma}_w - \frac{1}{2}\frac{d\bar{p}}{dz}\right)\log\left(\frac{R}{H+1}\right), \tag{15}$$

$$\bar{w}_R = R, \tag{16}$$

$$\bar{p}_s = \bar{p} + \left(\frac{\partial \bar{p}}{\partial Z}\right)^2 \frac{R^2-1}{4} + \frac{\partial \bar{p}}{\partial Z}\left(\dot{\gamma}_w - \frac{1}{2}\frac{d\bar{p}}{dz}\right)\log(R), \tag{17}$$

where $\dot{\gamma}_w$ is the strain rate at the wall and the mean pressure $\bar{p}$ is only a function of z. The underlined terms in Eqs. (15) and (17) turn out to be zero for the parabolic flow in a cylindrical tube with a constant pressure gradient. These terms, along with those in the linear stability analysis indicated later, result in the decrease in the transition Reynolds number due to the modification of the mean velocity profile and the pressure gradient. The stress balance conditions (14) are satisfied for

$$\bar{p} = \bar{p}_s - 1. \tag{18}$$

C. Linear stability analysis

In the linear stability analysis, small perturbations are imposed on the velocity and wall displacement fields of the form

$$v_i = \bar{v}_i + \tilde{v}_i(r)\exp[\iota k(z-ct)], \tag{19}$$

$$w_i = \bar{w}_i + \tilde{w}_i(R)\exp[\iota k(Z-ct)], \tag{20}$$

where k is the wave number and c is the wave speed. These are inserted into the conservation equations and linearized in the perturbations the fluid mass and momentum conservation equations,

$$r^{-1}d_r(r\tilde{v}_r) + \iota k\tilde{v}_z = 0, \tag{21}$$

$$(\mathrm{Re}/\Gamma)\iota k(\bar{v}_z-c)\tilde{v}_r = -d_r\tilde{p} + \left(d_r^2 + r^{-1}d_r - r^{-2} - k^2\right)\tilde{v}_r, \tag{22}$$

$$(\mathrm{Re}/\Gamma)[\iota k(\bar{v}_z-c)\tilde{v}_z + \tilde{v}_r d_r\bar{v}_z] = -\iota k\tilde{p} + \left(d_r^2 + r^{-1}d_r - k^2\right)\tilde{v}_z, \tag{23}$$

where $d_r \equiv (d/dr)$.

The incompressibility condition for the wall material, $\mathrm{Det}(\mathbf{F}) = 1$, reduces to

$$\iota k\tilde{w}_Z + R^{-1}d_R(R\tilde{w}_R) - \frac{d\bar{w}_Z}{dR}\iota k\tilde{w}_R = 0. \tag{24}$$

The momentum conservation equations for the wall material are

$$-\frac{\mathrm{Re}}{\Gamma}k^2c^2\tilde{w}_Z = -\iota k\tilde{p}_s - \frac{d\bar{p}}{dZ}\frac{1}{R}\frac{d(R\tilde{w}_R)}{dR} + \frac{\partial\bar{p}_s}{\partial R}\iota k\tilde{w}_R$$
$$+ \frac{1}{R}\frac{d(R\tilde{w}_Z)}{dR} - k^2\tilde{w}_Z, \tag{25}$$

$$-\frac{\mathrm{Re}}{\Gamma}k^2c^2\tilde{w}_R = -d_R\tilde{p}_s + \iota k\tilde{p}_s\frac{\partial\bar{w}_Z}{\partial R} - \frac{\partial\bar{p}_s}{\partial R}\left(\frac{\tilde{w}_R}{R} + \iota k\tilde{w}_Z\right)$$
$$+ \frac{\partial\bar{p}}{\partial Z}\left(d_R\tilde{w}_Z + \frac{\tilde{w}_R}{R}\frac{d\bar{w}_Z}{dR}\right)$$
$$+ \frac{d}{dR}\left[\frac{1}{R}\frac{d(R\tilde{w}_R)}{dR}\right] - k^2\tilde{w}_R. \tag{26}$$

The boundary conditions at $r = 0$ are the no normal velocity condition, $\tilde{v}_r = 0$ and the symmetry condition $d_r\tilde{v}_z = 0$, while the boundary conditions at $R = 1+H$ are the zero displacement conditions, $\tilde{w}_R = \tilde{w}_Z = 0$. At the perturbed interface $R = 1 + \tilde{w}_R$, the continuity of velocity and stress conditions are used. When the interfacial continuity of velocity conditions are written in terms of the fields at the unperturbed interface $R = 1$ using an expansion in $\tilde{w}_R$, we obtain

$$\tilde{v}_r = -\iota kc\tilde{w}_R, \tag{27}$$

$$\tilde{v}_z + \dot{\gamma}_w\tilde{w}_R = -\iota kc\tilde{w}_Z, \tag{28}$$

where $\dot{\gamma}_w$ is the strain rate at the wall. In the above equation, the second term on the left accounts for the variation in the mean velocity in the fluid due to the displacement of the surface.

The normal stress continuity equation is of the form

$$\mathbf{n}\cdot\sigma\cdot\mathbf{n} = \mathbf{n}\cdot\tau\cdot\mathbf{n}, \tag{29}$$

where the unit normal to the surface can be expressed, in the linear approximation as

$$\mathbf{n} = \mathbf{e}_R - \frac{\partial w_R}{\partial Z}\mathbf{e}_Z. \tag{30}$$

Using this, the normal stress balance equation, up to linear order in the perturbations, becomes

$$\tilde{\tau}_{rr} = \tilde{\sigma}_{RR}. \tag{31}$$

The equality of the mean shear stress at the interface has been used in simplifying the above condition. Expressed in terms of the displacement and velocity fields, the normal stress continuity is

$$-\tilde{p}_f + 2d_r\tilde{v}_r = -\tilde{p}_s + 2d_R\tilde{w}_R. \tag{32}$$

The tangential stress condition is discussed in some detail, since this is significantly altered by the modification of the velocity profile and pressure gradient due to tube deformation. In the tangential direction, the stress balance condition requires that

$$\mathbf{t}\cdot\tau\cdot\mathbf{n} = \mathbf{t}\cdot\sigma\cdot\mathbf{n}, \tag{33}$$

where the unit tangent to the surface, in the linear approximation, is given by

$$\mathbf{t} = \mathbf{e}_Z + \frac{\partial w_R}{\partial Z}\mathbf{e}_R. \tag{34}$$

Expressed in terms of components, and retaining terms up to linear order in the perturbations, the tangential stress balance can be written as

$$\tau_{zr} + \frac{\partial w_R}{\partial Z}(\tau_{rr} - \tau_{zz}) = \sigma_{ZR} + \frac{\partial w_R}{\partial Z}(\sigma_{RR} - \sigma_{ZZ}). \quad (35)$$

The above condition is applicable at the deformed interface. When expressed as a Taylor expansion about the undeformed interface $r = 1$, and considering terms up to linear order in the perturbations, we obtain

$$\tilde{\tau}_{zr} + \tilde{w}_R \frac{\partial \bar{\tau}_{zr}}{\partial r} + \iota k \tilde{w}_R(\bar{\tau}_{rr} - \bar{\tau}_{zz}) + \tilde{w}_R \frac{d\bar{\tau}_{zr}}{dr}$$
$$= \tilde{\sigma}_{ZR} + \iota k \tilde{w}_R(\bar{\sigma}_{RR} - \bar{\sigma}_{ZZ}). \quad (36)$$

Here we have included the variation of the mean shear stress with displacement in the fluid but have not included it for the solid, since the boundary conditions are applied at the unperturbed interface in the Eulerian description. There is no mean normal stress difference in the fluid, but there is a mean normal stress difference in the solid, which is given by

$$\bar{\sigma}_{RR} - \bar{\sigma}_{ZZ} = -\left[\frac{1}{R}\left(\dot{\gamma}_w - \frac{1}{2}\frac{d\bar{p}}{dz}\right) + \frac{R}{2}\frac{d\bar{p}}{dz}\right]^2. \quad (37)$$

This can be inserted into the stress balance equation to obtain

$$d_r\tilde{v}_z + \iota k \tilde{v}_r + \tilde{w}_R \frac{d\bar{\tau}_{zr}}{dr} + \frac{d\bar{p}}{dz} = d_R\tilde{w}_Z + \iota k \tilde{w}_R$$

$$+ d_R\tilde{w}_R \left[\frac{1}{R}\left(\dot{\gamma}_w - \frac{1}{2}\frac{d\bar{p}}{dz}\right) + \frac{R}{2}\frac{d\bar{p}}{dz}\right]$$

$$- \iota k \tilde{w}_R \left[\frac{1}{R}\left(\dot{\gamma}_w - \frac{1}{2}\frac{d\bar{p}}{dz}\right) + \frac{R}{2}\frac{d\bar{p}}{dz}\right]^2. \quad (38)$$

In the above equations, the underlined terms turn out to be zero for the parabolic flow in a tube with a constant pressure gradient; the difference in the results of the linear stability analysis for a cylindrical tube and that for a tube of varying cross section reported here is primarily due to these terms, especially the term proportional to the square of the fluid pressure gradient in Eq. (38).

The spectral collocation technique based on an expansion in Chebyshev polynomials is used to solve the linear stability equations [12]. The velocity field in the fluid and the displacement field in the gel are expanded in a series of Chebyshev polynomials, typically including 50–60 terms in the expansion, and the dispersion matrix is constructed from the values of the velocity and displacement fields and their derivatives at the nodes which are the zeros of the next-higher Chebyshev polynomial. Two of the rows of the dispersion matrix correspond to the boundary conditions at $r = 0$ for the velocity and $r = 1 + H$ for the displacement, while there are four rows for the boundary conditions at the interface $r = 1$. These are solved to obtain discrete eigenvalues. The numerical values of the lowest eigenvalues are insensitive to the number of basis functions used, provided the number is large (greater than about 50), though the total number of eigenvalues does depend on the number of basis functions used. A sufficiently large number of basis functions is used here, typically 50–60, so the magnitudes of the lowest eigenvalues do not change by more than 1% when the number of basis functions is increased by 10. The results of the numerical calculations have been validated against the previous linear stability analysis of Gaurav and Shankar [12] for the parabolic flows in a tube with a constant pressure gradient.

IV. RESULTS

The mean velocity profiles for a tube, in which the test section is fabricated using shear modulus 18 kPa, at a Reynolds number of 1025, are shown in Fig. 4(a). At all sections, we have verified that the predicted flow rates are invariant with axial distance; the variation in the flow rate at different axial locations is less than 0.1%. Figure 4(a) shows that the tube radius increases from the undeformed value of 600 μm to a

(a)

(b)
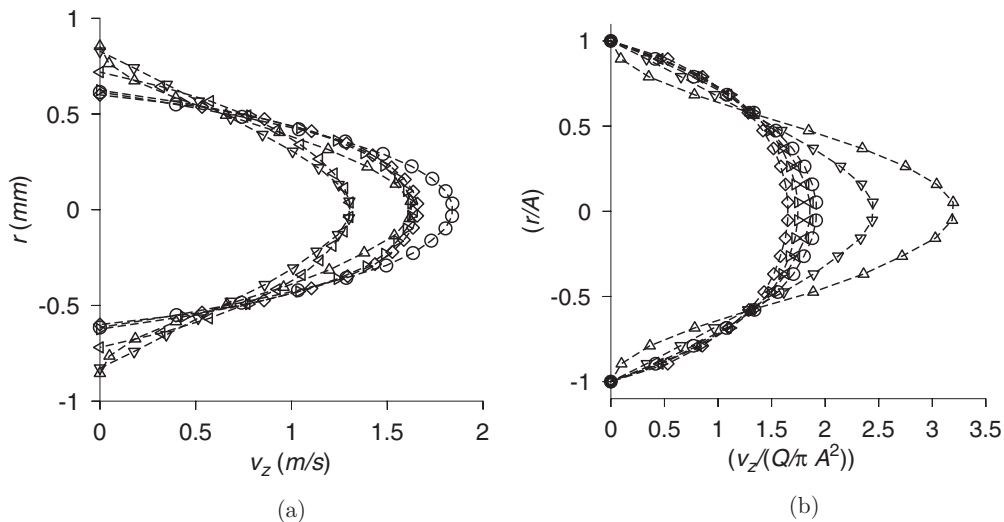
FIG. 4. The mean velocity $\bar{v}_z$ (m/s) as a function of the radius r (μm) (a) and the scaled mean velocity $[\bar{v}_z/(\pi Q/A^2)]$ as a function of the scaled radius (r/A) (b) for the flow in a tube of undeformed diameter 1200 μm in which the developing section is fabricated with shear modulus 18 kPa at a Reynolds number (based on mean diameter) of 1025 at distances $x = 0$ cm ($\circ$), 1 cm ($\triangle$), 3.5 cm (∇), 6 cm ($\triangleleft$), 8.8 cm ($\triangleright$), and at 9 cm ($\diamond$) from the joint between the developing and test sections. Here A is the deformed radius at the location z.
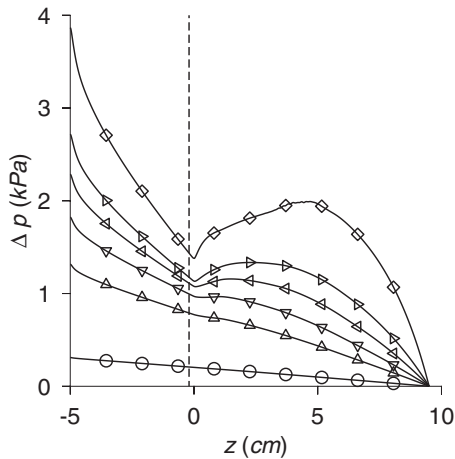
FIG. 5. The pressure as a function of axial distance z for a tube in which the developing section is made of PDMS gel with shear modulus 18 kPa for Reynolds numbers 126 ($\circ$), 521 ($\triangle$), 716 ($\triangledown$), 888 ($\triangleleft$), 1025 ($\triangleright$), and 1240 ($\diamond$). The joint between the developing and test sections is at $z = 0$, and the vertical line shows the location of the pressure transducer.

maximum of about 854 μm about 1 cm downstream of the entrance to the test section at the Reynolds number of 1025. This results in a significant distortion of the mean velocity profile. The distortion is better visualized in the graph of the scaled mean velocity $[\bar{v}_z/(Q/\pi A^2)]$ as a function of the scaled radius (r/A) in Fig. 4(b), where A is the radius of the deformed tube at the axial location z. In the diverging section, the velocity at the center of the tube is significantly higher than the value of 2 expected for a parabolic profile, whereas the velocity is more pluglike in the downstream converging section where the scaled mean velocity is lower than the value of 2 expected for a parabolic profile.

The pressure variation along the axial length is shown for a tube with test section made of polymer gel with shear modulus 18 kPa at different Reynolds numbers in Fig. 5. A linear variation of pressure with downstream distance, expected for the laminar flow through a cylindrical tube, is observed at low Reynolds number. However, as the Reynolds number increases, there is a significant variation in the pressure gradient due to the tube wall deformation. The pressure decreases linearly with distance in the hard developing section for $z < 0$, but there is an increase in the pressure in the diverging section for z less than about 3 cm in the test section and a subsequent decrease in pressure in the downstream converging section.

The pressure difference between the pressure transducer (vertical line in Fig. 5) and the outlet is compared with experimental results for tubes in which the test section is made of gels of different shear moduli in Fig. 6. For a hard gel in which the test section is made with shear modulus 0.5 MPa, the flow simulations predict a linear increase of pressure with distance, and these are in agreement with experiments up to a Reynolds number of about 2000, at which the rigid tube transition takes place. As the tube walls are made softer, the experimental pressure difference deviates from the theoretical value at an increasingly lower Reynolds number,

and the minimum Reynolds number is about 800 for the softest gel with shear modulus 18 kPa. The Reynolds number at which there is a difference between the theoretical and experimental pressure difference also coincides, within about 5%, with that at which transition is observed in experiments. It should be noted that the flow simulations only predict laminar velocity profiles, since we have not used any turbulence model in the simulations, even though the velocity profile differs substantially from a parabolic velocity profile in some cases due to tube deformation, as shown in Fig. 4. This suggests that the cause of the difference in the pressure drop between experiments and simulations is because the transition in experiments results in a significantly higher pressure gradient in comparison to the laminar flow captured by the flow simulations.

The mean velocity and pressure gradients determined from the flow simulations are used to determine the wave speed as a function of wave number in the linear stability analysis. The results for the imaginary part of the wave speed for the least stable and most unstable modes are shown in Fig. 7 for three different Reynolds numbers for a tube in which the wall is made of soft gel with shear modulus 18 kPa. All of these curves have a some common features. The value of c_i is negative in the low wave number limit, indicating that perturbations are stable. As k increases, the magnitude of c_i first increases, reaches an intermediate maximum, and then decreases again. Upon further increase in k, the magnitude increases from a minimum and approaches the $c_i = 0$ axis at high wave number. The value of c_i is negative at all locations at a low Reynolds number of 521. As the Reynolds number increases, the value of c_i at the intermediate maximum increases and approaches the $c_i = 0$ axis at the outlet ($x = 9.5$ cm) at a Reynolds number of 716. Upon further increase in the Reynolds number to 888, the value of c_i is positive at the intermediate maximum, indicating the presence of unstable modes. Since this intermediate maximum has the largest value for unstable modes, the value of this intermediate maximum and the corresponding wave number are analyzed further as a function of Reynolds number and downstream position.

The maximum value of the imaginary part of the wave speed from the linear stability analysis, calculated using the velocity profile and pressure gradient at different downstream locations, is shown as a function of Reynolds number in Figs. 8(a), 9(a), and 10(a) for tubes made with different wall elasticity moduli. The imaginary part of the wave speed first becomes positive at a Reynolds number of 888 for the tube with shear modulus 18 kPa, at a Reynolds number of 1217 for shear modulus 25 kPa, and at Reynolds number of 1439 for shear modulus 35 kPa. In all cases, the maximum c_i first becomes positive at the downstream end of the tube, at a distance between 9 and 9.5 cm from the inlet, and not near the inlet of the soft part of the tube where the deformation is a maximum. It should also be noted that the downstream section of the tube is a converging section, where the flow is accelerating and the flow is more pluglike in comparison to a parabolic flow, as shown in Fig. 4. There is a sharp increase in the maximum value of c_i in the upstream diverging section at a Reynolds number of 1139 for the tube with shear modulus 18 kPa and 1582 for the tube with shear modulus 25 kPa, but this is at a significantly higher Reynolds number than that at which the flow is predicted to
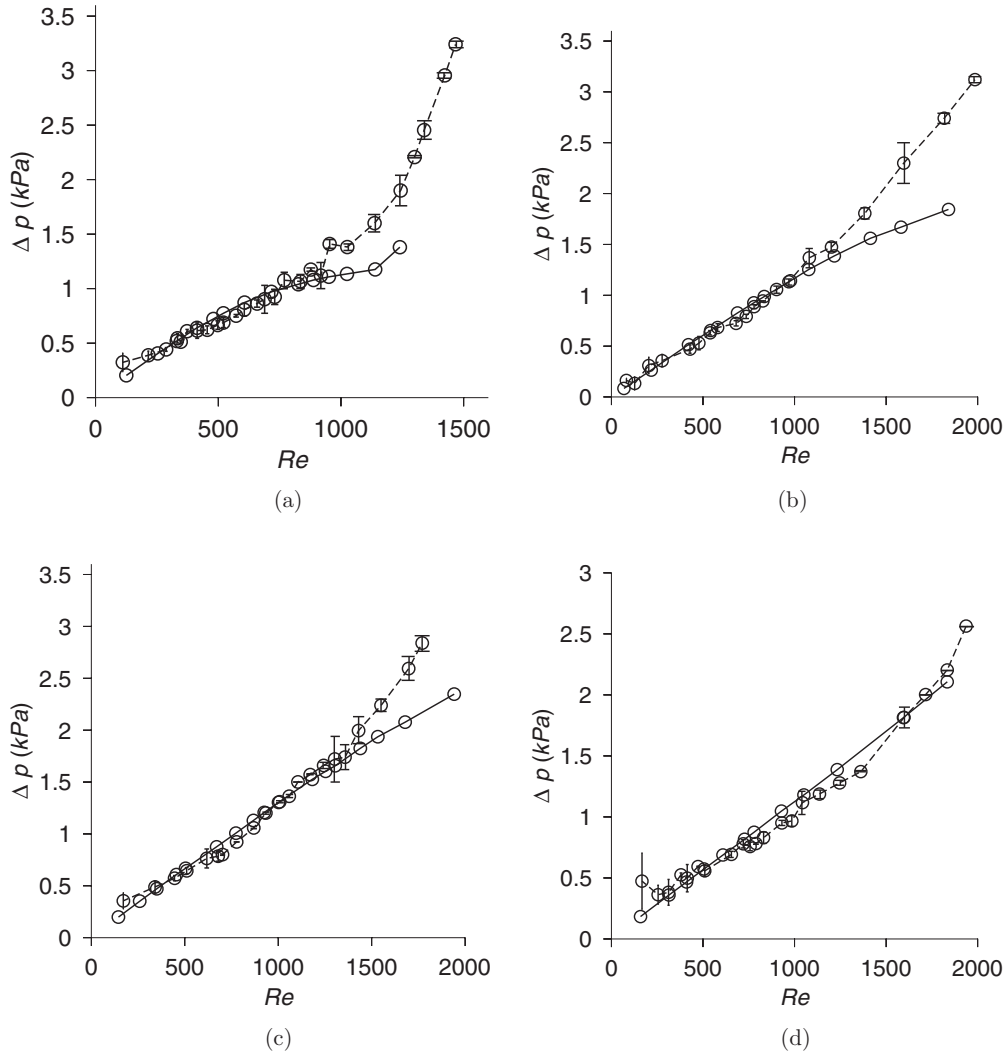
FIG. 6. The pressure difference between the pressure transducer and the tube outlet for tubes in which the developing section is made of soft gel with shear modulus 18 kPa (a), shear modulus 25 kPa (b), and shear modulus 35 kPa (c), and a hard tube with shear modulus 0.5 MPa (d). The dashed lines show the experimental results, while the results from flow simulations are shown by the solid lines.

go unstable at the downstream section. This sharp increase in c_i at the upstream location is not observed for a gel with shear modulus 35 kPa.

The wave number of the most unstable mode is shown as a function of downstream location in Figs. 8(b), 9(b), and 10(b). This figure indicates that the wavelength of the most unstable modes is about 40 times larger than the radius of the tube, and it does not show a significant variation as the perturbations become unstable at the downstream end of the tube. However, for gels with shear modulus 18 kPa and 25 kPa there is a sharp decrease in the wavelength corresponding to the instability in the upstream section.

The validity of the parallel flow approximation can now be examined. The parallel flow approximation is valid when the wavelength of the most unstable mode is much smaller than the flow development length, which can be considered as the ratio of the local tube radius and the wall slope. The wall slope at different downstream locations, calculated from the tube cross sections of the type shown in Fig. 1 using a fifth-order

polynomial fit for the wall radius, is shown in Fig. 11. The slope of the wall has a maximum magnitude of about 4–5% at the upstream expanding section for Reynolds numbers greater than 1000. However, at the downstream section where the instability is first observed, the slope of the wall is less than 0.5% at the transition Reynolds number of about 1025. This indicates that the flow development length is about 200 times the tube radius in the downstream section. In comparison, Figs. 8 to 10 show that the wave number of the most unstable waves is about 0.15, which implies that the wavelength of the most unstable modes is only about 40 times the tube radius. Therefore, the parallel flow approximation is valid in the downstream converging section where the flow becomes unstable, though it may not be valid in the upstream diverging section where the flow is found to be stable.

Insight into the physical mechanism of the instability is obtained from the eigenfunctions for the fluctuations in the streamwise velocity $\tilde{v}_z$, scaled by its value at the wall $r = 1$, are shown as a function of radial position at two different
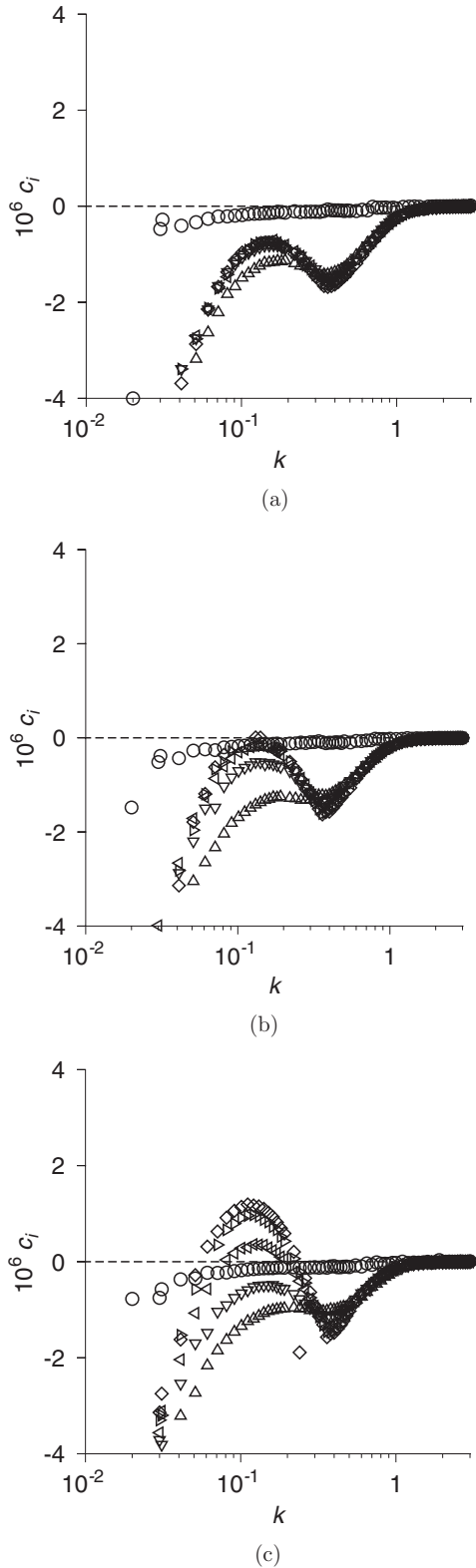
FIG. 7. The imaginary part for the wave speed c_i for the mode with the largest c_i as a function of the wave number k for the flow through a tube with wall made of gel with shear modulus 18 kPa at Reynolds numbers 521 (a), 716 (b), and 888 (c) at different downstream locations x from the inlet of the soft section, $x = 0$ (○), $x = 1$ cm, (△), $x = 3.5$ cm (▽), $x = 6$ cm (◁), and $x = 8.8$ cm (▷) and at the outlet $x = 9.5$ cm (◇).

downstream locations in Fig. 12(a). The eigenfunction for the velocity is nonzero at the wall. This differs substantially from a rigid tube, where the eigenfunction has to be zero due to no-slip condition. This indicates that wall motion is involved in destabilizing the flow, which differs markedly from transition in a rigid channel. The velocity fluctuations are confined to a thin layer near the wall of the tube, confirming that the instability is due to the wall-mode instability mechanism. The theoretical analysis of the wall-mode instability mechanism has been discussed extensively before [22–24], and so we do not repeat the discussion here but we note that the mechanism of instability, which is the transport of energy from the mean flow to the fluctuations due to the shear work done at the interface, differs markedly from the transition mechanism in a rigid tube. The salient features of the instability, the confinement of the velocity fluctuations to a thin region of thickness $Re^{-1/3}$ near the wall, and the velocity fluctuations are maximum at the wall are all observed in Fig. 12. A definite scaling for the wall layer thickness as a function of the Reynolds number could not be obtained, but the confinement of the disturbances to a region near the wall indicates that this is the wall-mode instability and not the inviscid instability in which disturbances are confined to an internal critical layer. The Fig. 12(a) also rules out the near wall turbulent bursting (responsible for transition in rigid tubes) as the mechanism here, since that would involve a maximum in the velocity fluctuations close to, but not at, the wall. The displacement in the wall is also confined to a region near the fluid-wall interface, and the displacement decreases to zero within a distance of about 1.5 times the tube radius. For this reason, the boundary conditions on the displacement field at the outer boundary do not significantly affect the eigenfunctions at the outer boundary.

There are two reasons for the decrease in the transition Reynolds number predicted by the linear stability analysis. The first is a modification of the mean velocity profile which results in a lower velocity gradient at the wall in the diverging section and a higher velocity gradient at the wall in the converging section, in comparison to a parabolic profile for the same flow rate. The change in the slope at the wall can be estimated on the basis of the scaling analysis [3]. If the Reynolds number is Re and a slope of the wall is α, the modification of the mean flow velocity is $O(Re\alpha)$. This could be large even though the slope of the wall α is small. A simple scaling analysis in the limit of high Reynolds number indicates that the velocity gradient at the wall is $(Re\alpha)^{1/2}$, higher than that for a parabolic flow for the same flow rate and tube radius. So the slope could be much higher than that predicted based on a parabolic profile. The velocity gradient at the wall at different downstream locations is compared with the velocity gradient for a parabolic flow with the same flow rate in Fig. 13. It is observed that the velocity gradient at the downstream section could be larger, by a factor of 2 in comparison to that for a parabolic flow for the transition Reynolds number of about 1025. Thus, the increase in the strain rate is not adequate to explain the decrease of the transition Reynolds number by a factor of 10. The other factor in the linear stability analysis which differs from that for a parabolic flow is the local pressure gradient, shown in Fig. 5. The local pressure gradient at different downstream
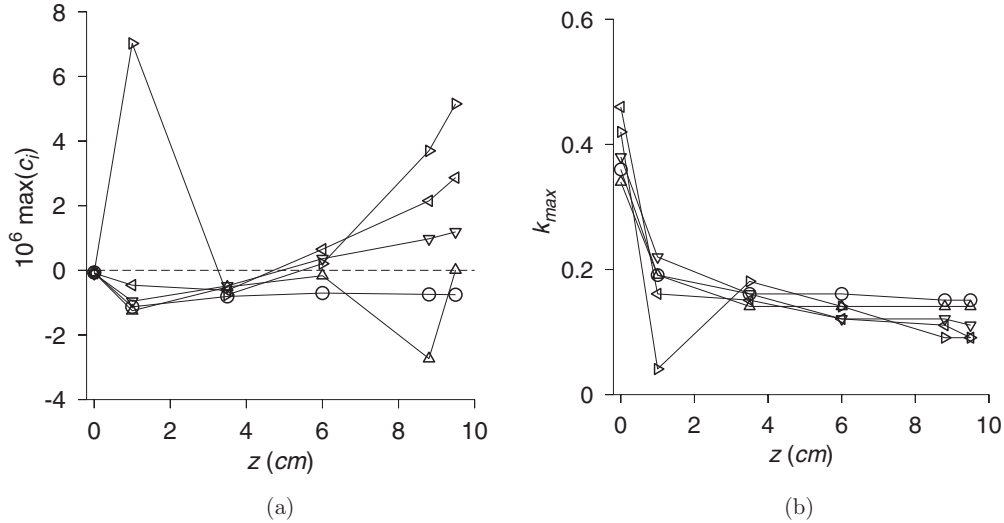
FIG. 8. The maximum of the imaginary part of the wave speed c_i (a) and the scaled wave number of the most unstable mode k_{max} (b) as a function of downstream distance x from the entrance to the soft section for gels in which the soft wall is made with shear modulus 18 kPa for Reynolds numbers 521 ($\circ$), 716 ($\triangle$), 888 (∇), 1025 ($\triangleleft$), and 1139 ($\triangleright$).

sections is compared with the ratio of the pressure difference and tube length across the soft section in Fig. 14. While the pressure gradient is approximately a constant negative value for low Reynolds numbers less than about 200 (not shown in Fig. 14), at higher Reynolds number, the pressure gradient first increases in the expanding section and then decreases in the converging section downstream. As shown in Fig. 14, the magnitude of the pressure gradient in the downstream accelerating flow could be larger, by a factor of 4–5, than the difference in pressure across the ends divided by the length of the tube. This results in a significant modification in the shear stress condition at the interface, Eq. (38), since the boundary condition contains a term that is proportional to the square of the pressure gradient. Since the mechanism of destabilization

of the wall-mode instability is the transport of energy from the mean flow to the fluctuations due to the shear work done at the interface [22,23], this modification of the shear stress condition significantly reduces the transition Reynolds number. Due to the quadratic dependence of the boundary condition (38) on the pressure gradient, a combination of the large increase in the pressure gradient and the relatively smaller increase in the wall strain rate tends to destabilize the flow at a Reynolds number 10 times smaller than that predicted for a parabolic flow in a tube with a constant pressure gradient. We have carried out calculations using the parallel flow approximation where the strain rate is determined from the actual velocity profile, and the pressure gradient is assumed to be the difference in pressure across the soft section of the tube divided by its length. With
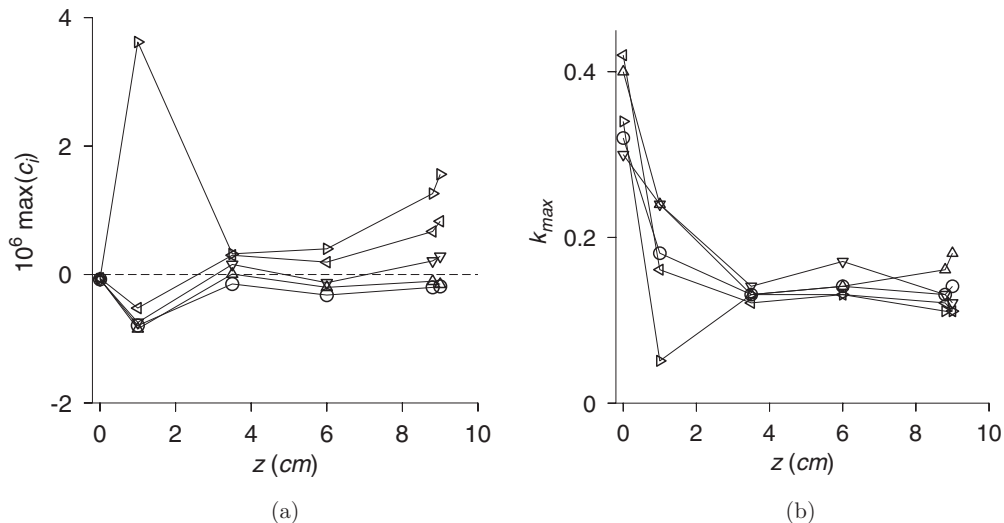
FIG. 9. The maximum of the imaginary part of the wave speed c_i (a) and the scaled wave number of the most unstable mode k_{max} (b) as a function of downstream distance x from the entrance to the soft section for gels in which the soft wall is made with shear modulus 25 kPa for Reynolds numbers 978 ($\circ$), 1077 ($\triangle$), 1217 (∇), 1414 ($\triangleleft$), and 1582 ($\triangleright$).
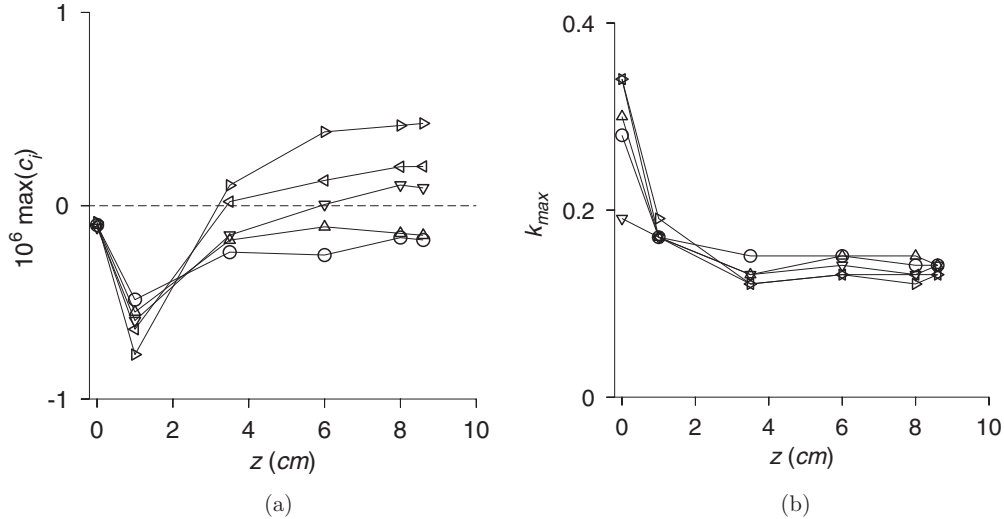
FIG. 10. The maximum of the imaginary part of the wave speed c_i (a) and the scaled wave number of the most unstable mode k_{max} (b) as a function of downstream distance x from the entrance to the soft section for gels in which the soft wall is made with shear modulus 35 kPa for Reynolds numbers 1182 ($\circ$), 1305 ($\triangle$), 1439 (∇), 1533 ($\triangleleft$), and 1679 ($\triangleright$).

this approximation, the transition Reynolds number decreases by very little, indicating that the increase in the magnitude of the pressure gradient in the downstream section is crucial for destabilizing the flow.

The transition Reynolds number observed by different methods in the experiments is compared with the theoretical predictions in Table I. The Reynolds number at which the maximum c_i becomes positive is in good agreement with that at which there is a divergence between the experimental and theoretical pressure differences in Fig. 6. Both the location of the instability (downstream end of the tube) and the Reynolds number for the instability are in quantitative agreement with the Reynolds number at which dye-stream breakup and wall oscillations are observed in the experiment. The Reynolds number for transition from friction factor measurements is

in agreement, within about 10%, with that from the other methods.

In Table I, the results of the present linear stability analysis (column V) are also compared with the results of a previous linear stability analysis [12] carried out for a parabolic flow in a cylindrical tube with the same same flow rate as that in the experiments and with the same diameter as that at the downstream location where the instability is observed (column VI). Here we see that the Reynolds number predicted for a linear instability is about an order of magnitude higher than that for the present analysis in a deformed tube and is even higher than the Reynolds number of 2100 where transition is observed in experiments in a rigid tube. (Note that linear stability analysis predicts that a parabolic flow in a rigid tube is stable at all Reynolds numbers, and there is no linear instability.)

The present analysis has successfully resolved the discrepancy of about an order of magnitude between experiments and
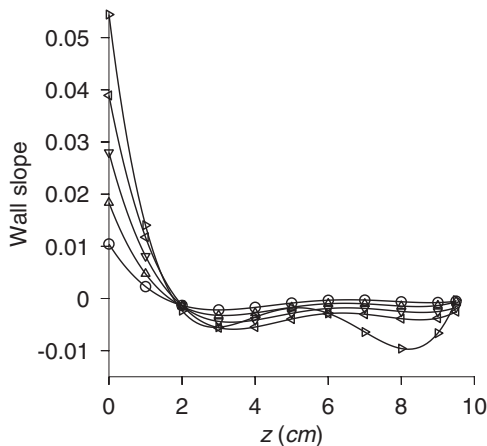
FIG. 11. The slope of the wall as a function of downstream distance z for tubes in which the soft wall is made with shear modulus 35 kPa for an average Reynolds number of 521 ($\circ$), 716 ($\triangle$), 888 (∇), 1025 ($\triangleleft$), and 1139 ($\triangleright$).

TABLE I. The transition Reynolds number from the friction factor measurements (column I), dye-stream measurements (column II), wall oscillations observed from laser scattering (column III), all from Verma and Kumaran [3], and the Reynolds number for divergence between the experimental pressure drop and that from numerical simulations (IV) and the Reynolds number at which the maximum value of c_i becomes positive at the downstream location (V), and the theoretical prediction for a parabolic flow with a constant pressure gradient of equal flow rate in a flexible tube of the same shear modulus and diameter (VI), as a function of the shear modulus of the soft wall G and the parameter $\Sigma = \rho G A^2 / \mu^2$, where A is the undeformed tube radius and μ is the fluid viscosity.

G (kPa)	Σ	I	II	III	IV	V	VI
18	9.6×10^6	834	930	903	877	888	7840
25	12.7×10^6	1085	1190	1116	1202	1217	11230
35	15.3×10^6	1355	1400	1470	1429	1439	14540
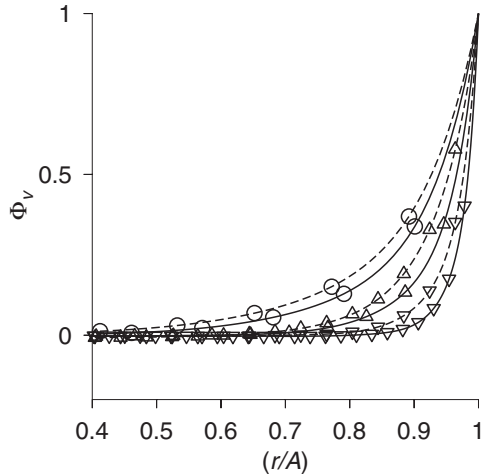
(a)
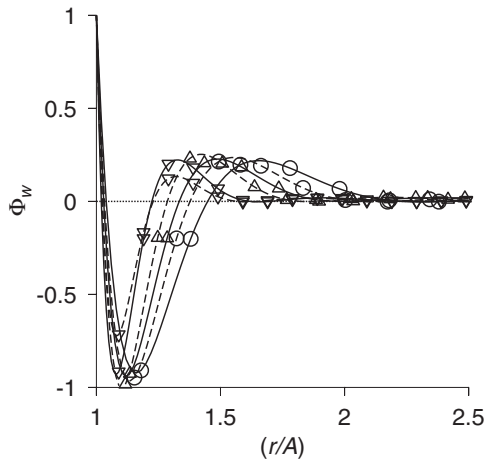
(b)

FIG. 12. The scaled streamwise fluid velocity fluctuations $\Phi_v = \tilde{v}_z / \tilde{v}_z|_{r=A}$ (a) and the scaled streamwise displacement fluctuations in the solid $\Phi_u = \tilde{w}_Z / \tilde{w}_Z|_{r=A}$ (b) as a function of r/A at two downstream locations 8.8 cm from the entrance of the soft section (solid line) and 9.5 cm from the entrance of the soft section (dashed line) for tube with soft section made of gel with shear modulus 18 kPa at Re = 888 (○), tube with soft section made of gel with shear modulus 25 kPa and Re = 1217 (△), and for a tube with soft section made of gel with shear modulus 35 kPa and Re = 1419 (▽).

theory for the transition Reynolds number for the flow through a flexible tube. The reduction in the transition Reynolds number due to modification in the pressure gradient and velocity profile in the converging section seems to be a generic feature of the flow in flexible conduits, as shown by the present analysis for the flow in a flexible tube and the previous analysis [4] for the flow in a flexible channel. To place the present result in context, it should be noted that the minimum elasticity modulus of soft polymer gels is of the order of 1–10 kPa, and it is difficult to make gels with a lower shear modulus since the cross-link density is not sufficient to hold the material together. For such materials, linear stability analysis predicts
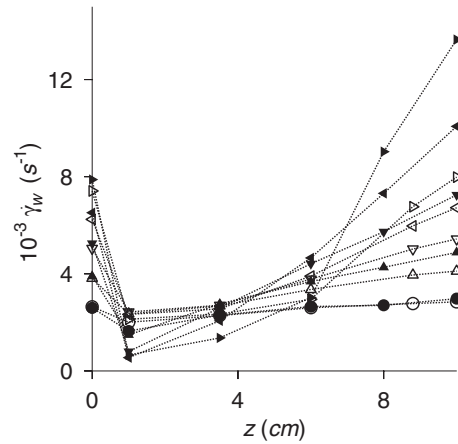
FIG. 13. The velocity gradient at the wall from the simulations for the base flow (solid symbols) and the velocity gradient for a parabolic flow with the same flow rate (open symbols) as a function of downstream distance z for tubes in which the soft wall is made with shear modulus 35 kPa for an average Reynolds number of 521 (○), 716 (△), 888 (▽), 1025 (◁), and 1139 (▷). The lines are drawn to provide visual guidance.

that the transition Reynolds is higher than the Reynolds number of 2100 where transition is experimentally observed in a rigid tube. (Note that linear stability studies indicate that the flow in a rigid tube is stable at all Reynolds numbers, and there is no linear instability.) In the absence of this reduction due to tube convergence and flow modification, it would not have been possible to observe a reduction in the transition Reynolds number in experiments. This fortuitous reduction in the transition Reynolds number makes it feasible to use wall flexibility as a practical means of inducing a transition to turbulence and thereby significantly enhancing mixing [4].
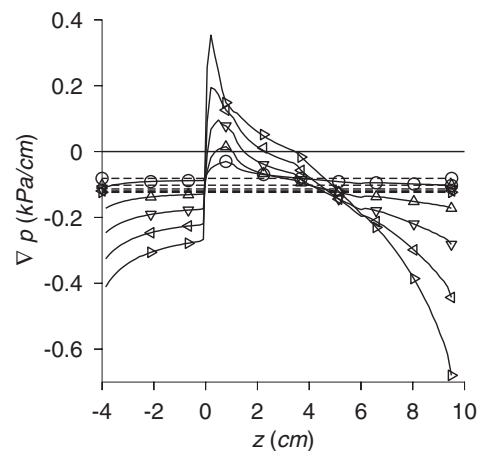
FIG. 14. The actual gradient from the simulations for the base flow (solid lines) and the pressure difference between the entrance of the soft section ($z = 0$ cm) and the outlet ($z = 14.5$ cm) divided by the tube length (9.5 cm) as a function of downstream distance z (dashed lines) for tubes in which the soft wall is made with shear modulus 35 kPa for an average Reynolds number of 521 (○), 716 (△), 888 (▽), 1025 (◁), 1139 (▷).

ACKNOWLEDGMENT

[1] G. M. Whitesides, The origins and the future of microfluidics, Nature **442**, 368 (2006).

[2] A. J. de Mello, Control and detection of chemical reactions in microfluidic systems, Nature **442**, 394 (2006).

[3] M. K. S. Verma and V. Kumaran, A dynamical instability due to fluid-wall coupling lowers the transition reynolds number in the flow through a flexible tube, J. Fluid Mech. **705**, 322 (2012).

[4] M. K. S. Verma and V. Kumaran, A multifold reduction in the transition reynolds number, and ultra-fast mixing, in a microchannel due to a dynamical instability induced by a soft wall, J. Fluid Mech. **727**, 407 (2013).

[5] V. C. Patel and M. R. Head, Some observations on skin friction and velocity profiles in fully developed channel flows, J. Fluid Mech. **38**, 181 (1969).

[6] P. G. Drazin and W. H. Reid, *Hydrodynamic Stability* (Cambridge University Press, Cambridge, UK, 1981).

[7] V. Kumaran, G. H. Fredrickson, and P. Pincus, Flow induced instability at the interface between a fluid and a gel at low Reynolds number, J. Phys. France II **4**, 893 (1994).

[8] V. Kumaran, Stability of the viscous flow of a fluid through a flexible tube, J. Fluid Mech. **294**, 259 (1995).

[9] R. M. Thaokar, V. Shankar, and V. Kumaran, Effect of tangential interface motion on the viscous instability in fluid flow past flexible surfaces, Euro. Phys. J. B **23**, 533 (2001).

[10] P. P. Chokshi and V. Kumaran, Weakly nonlinear analysis of viscous instability in flow past a neo-Hookean surface, Phys. Rev. E **77**, 056303 (2008).

[11] V. Gkanis and S. Kumar, Stability of pressure driven creeping flows in channels lined with a nonlinear elastic solid, J. Fluid Mech. **524**, 357 (2005).

[12] Gaurav and V. Shankar, Stability of fluid flow through deformable neo-Hookean tubes, J. Fluid Mech. **627**, 291 (2009).

[13] Gaurav and V. Shankar, Stability of pressure-driven flow in a deformable neo-Hookean channel, J. Fluid Mech. **659**, 318 (2010).

[14] V. Shankar and V. Kumaran, Weakly nonlinear stability of viscous flow past a flexible surface, J. Fluid Mech. **434**, 337 (2001).

[15] P. P. Chokshi and V. Kumaran, Weakly nonlinear stability analysis of a flow past a neo-Hookean solid at arbitrary Reynolds numbers, Phys. Fluids **21**, 014109 (2009).

[16] V. Kumaran and R. Muralikrishnan, Spontaneous growth of fluctuations in the viscous flow of a fluid past a soft interface, Phys. Rev. Lett. **84**, 3310 (2000).

[17] R. Muralikrishnan and V. Kumaran, Experimental study of the instability of the viscous flow past a flexible surface, Phys. Fluids **14**, 775 (2002).

[18] M. D. Eggert and S. Kumar, Observations of instability, hysteresis, and oscillation in low-Reynolds-number flow past polymer gels, J. Colloid Interface Sci. **278**, 234 (2004).

[19] A. Shrivastava, E. L. Cussler, and S. Kumar, Mass transfer enhancement due to a soft elastic boundary, Chem. Eng. Sci. **63**, 4302 (2008).

[20] V. Kumaran, Stability of an inviscid flow in a flexible tube, J. Fluid Mech. **320**, 1 (1996).

[21] V. Shankar and V. Kumaran, Stability of non-axisymmetric modes in a flexible tube, J. Fluid Mech. **407**, 291 (2000).

[22] V. Shankar and V. Kumaran, Asymptotic analysis of wall modes in a flexible tube revisited, Eur. Phys. J. B **19**, 607 (2001).

[23] V. Kumaran, Stability of wall modes in a flexible tube, J. Fluid Mech. **362**, 1 (1998).

[24] V. Shankar and V. Kumaran, Stability of wall modes in the flow past a flexible surface, Phys. Fluids **14**, 2324 (2002).

[25] J. L. Sutterby, Finite difference analysis of viscous laminar converging flow in conical tubes, Appl. Sci. Res. A **15**, 241 (1965).

[26] V. Gkanis and S. Kumar, Instability of creeping flow past a deformable wall: The role of depth-dependent modulus, Phys. Rev. E **73**, 026307 (2006).

[27] V. Shankar and V. Kumaran, Stability of non-parabolic flows in a flexible tube, J. Fluid Mech. **395**, 211 (1999).